Metall. Res. Technol. **122**, 601 (2025)

https://doi.org/10.1051/metal/2025075

Metallurgical Research & Technology

Available online at:
www.metallurgical-research.org

Special Issue on 'Advances in Powder Technologies: Highlights from EuroPM2025', edited by Efrain Carreño-Morelli, Elena Gordo and Lars Nyborg

ORIGINAL ARTICLE OPEN ACCESS

Short-loop recycling of elevator motor magnets by hydrogen decrepitation and FAST sintering

Miguel Lagos[1,*], Blanca Luna Checa Fernández[1], Iñaki Leizaola[1], Jon Mikel Sanchez[1], Iñigo Agote[1], Gaizka Almandoz[2], Javier Poza[2], and Ana Escalada[3]

[1] TECNALIA, Basque Research and Technology Alliance (BRTA), Donostia 2009, Spain
[2] Mondragon Unibertsitatea, Faculty of Engineering, Arrasate 20500, Spain
[3] Orona S. Coop, Hernani, 20120, Spain

Received: 23 April 2025 / Accepted: 30 July 2025

Abstract. The increasing demand for permanent magnets based on Rare Earths (RE) in Europe, driven by the electrification of mobility and the growth of renewable energy technologies, poses significant supply risks due to the dependence on imports from China. With less than 1% of RE magnets recycled in the EU and no established remanufacturing value chain, there is a pressing need to enhance strategic autonomy in REs. The European Union's commitment to a circular economy requires innovative solutions to address this complex challenge. This work presents a short-loop recycling process for RE magnets, where magnets are converted into powder through hydrogen decrepitation and subsequently re-converted into new magnets through FAST sintering. This innovative approach enables the recovery of high-quality RE magnets, reducing waste and the demand for primary materials. The process is demonstrated through a case study on elevator motors, a key application where RE magnets play a critical role.

Keywords: magnets / recycling / fast sintering / rare earth

1 Introduction

The global demand for RE magnets has been steadily increasing due to their critical role in modern electric motor rotors and a growing range of high-tech applications. However, China has been the dominant producer of these magnets, accounting for more than 90% of global production over the last decade [1], and has led the production of rare-earth elements since the 1980s [2,3]. This poses a geopolitical risk to supply chains for Western countries [4]. Additionally, the extraction and purification of rare-earth elements have severe environmental impacts [5,6].

As the use of RE magnets continues to grow, the volume of discarded magnets is also rising rapidly, while less than 1% are being recycled today [7]. Developing sustainable recycling methods is crucial for reducing reliance on primary rare-earth extraction and mitigating its environmental impact. This study investigates the feasibility of a low-pollution, energy-efficient, and cost-effective recycling approach that utilizes Spark Plasma Sintering (SPS) to consolidate new magnets from recycled powder obtained via Hydrogen Decrepitation (HD) of scrap magnets. Hydrogen decrepitation consist of placing discarded magnets in a hydrogen-rich environment, causing the material to absorb hydrogen and break down into fine powder due to the volumetric expansion that takes place during the hydrogenation of the Nd-rich and $Nd_2Fe_{14}B$ matrix phase [8,9]. Therefore, hydrogen serves as an efficient processing agent for selectively extracting and recycling RE magnets from end-of-life (EOL) waste streams [10]. Life Cycle Analysis (LCA) has shown that hydrogen processing of magnets scraps reduces energy consumption for producing re-sintered magnets by approximately 80–90% compared to primary manufacturing [11].

Spark Plasma Sintering (SPS) is an advanced consolidation technique that enables precise control over sintering kinetics. Unlike conventional sintering or hot pressing, SPS utilizes an electric current (AC, DC, or pulsed) that passes through both the powder and the die, while simultaneously applying uniaxial pressure. This method facilitates the production of highly dense samples with controlled grain growth and reduced processing time. Prior research has demonstrated that SPS is well-suited for consolidating RE magnets [12,13].

In this study, we first outline the characteristics of the precursor material and the selected recycling process, which combines HD and SPS. We then present the

* e-mail: miguel.lagos@tecnalia.com

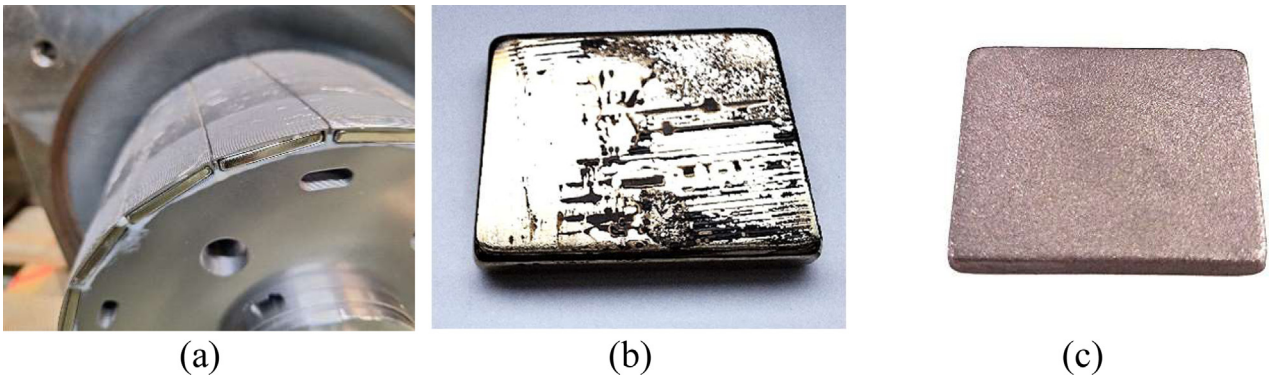

Fig. 1. (a) Elevator motor rotor with NdFeB magnets, (b) NdFeB EM-magnet after demagnetization treatment, and (c) EM-magnet after coating removal.

structural, microstructural, and magnetic properties of the consolidated magnets. Finally, we analyze the results and offer insights for future improvements, emphasizing the potential for optimizing this recycling process to make it not only efficient but also low-energy, cost-effective, and economically viable for large-scale implementation.

2 Experimental procedure

The raw material for this study consisted of NdFeB magnets sourced from elevator motor rotors (Orona S. Coop.), referred to as EM-magnets. The magnets were bonded to electrical steel plates using adhesive. To extract the magnets, a thermal cycle was employed with the dual purpose of removing the adhesive and demagnetizing the magnets. The thermal treatment was conducted at 400 °C for 2 h in an argon atmosphere. Following the thermal cycle, the magnets were manually extracted. The surface coating of Ni-Cu-Ni was subsequently removed using sandblasting. Figure 1 shows the NdFeB magnets within the rotor, after the demagnetization treatment and after the elimination of the coating. Residual pyrolized adhesive, visible on the magnets in Figure 1b, is a byproduct of the thermal treatment in argon. These residuals are removed along with the Ni-Cu-Ni coating during the sandblasting process.

The demagnetized and cleaned magnets were placed in a sealed vessel for the hydrogen decrepitation (HD) process. To ensure an inert atmosphere, the vessel underwent alternate purging with argon and vacuum, followed by pressurization to the desired hydrogen pressure. A series of hydrogen decrepitation (HD) experiments were conducted to study and optimize the process parameters for powder production and their subsequent effect on the properties of recycled magnets. Initially, a set of tests was performed to analyze the effect of initial hydrogen pressure on hydrogen absorption behavior. For this purpose, hydrogen pressures ranging from 3 to 50 bar were evaluated. In each case, after reaching the target pressure, the hydrogen inlet was closed, and the pressure drop was recorded to monitor the hydrogen uptake. All these tests were carried out using 20 g of magnet material, with the protective coating removed beforehand.

Subsequently, to produce HD powders at different pressures for further processing, two selected hydrogen pressures (3 and 20 bar) were maintained throughout the entire reaction time (ranging from 1 to 4 h). The resulting hydrogenated powders were sieved to a particle size below 425 μm, achieving 100% material recovery in powder form. These powders are designated as HD-3 and HD-20, respectively.

The effect of hydrogen pressure was studied not only at the powder level but also on the properties of the final recycled magnets obtained after consolidation via SPS. To more accurately understand the influence of residual hydrogen on this process, the HD powders were subjected to a high-temperature degassing cycle under high vacuum (furnace IPSEN VFCK 124HV). The temperature was increased slowly at a rate of 3 °C/min until exceeding 600 °C, achieving a recovery of vacuum levels below 10^{-4} mbar. The degassed powders are referred to as HD-D-3 and HD-D-20.

All powder handling and sample preparation were performed under an argon atmosphere in a glove box, maintaining oxygen levels below 5 ppm and moisture below 1 ppm to prevent contamination and ensure consistency in the results.

Sintering was performed with an SPS furnace (model S8451, FCT) under vacuum (4 mbar) and a constant 50 MPa of uniaxially applied pressure. The HD-D powder samples were placed into a graphite die, with boron nitride applied to the punches and/or the graphite foil inserted between the matrix and the powder. This configuration was used to ensure effective processing and prevent sample contamination or sticking during the sintering process. The SPS was temperature-controlled by means of a pyrometer that measures the temperature inside the graphite punch. The temperature was then increased to the selected temperature (studied temperatures between 750 and 1075 °C) at a rate of 80 °C/min and held for a duration of 2 min. After the sintering process was finished, the graphite spacers and pressing tools with the sample were cooled to room temperature by means of cooling water circulating through the electrodes. Prior to the geometrical density measurements, the graphite foil was removed from the surface of the samples using a SiC grinding paper.

Table 1. Chemical composition and impurity content of EM-magnets.

Sample	(wt.%)								(ppm)			
	Nd	Pr	Dy	Fe	Co	B	Cu+Ga+Al	Total RE	C	O	N	H
EM- magnet	20.2	7.0	1.5	65	1.0	1.0	0.79	28.7	790 ± 20	800 ± 100	490 ± 30	7.3 ± 0.4

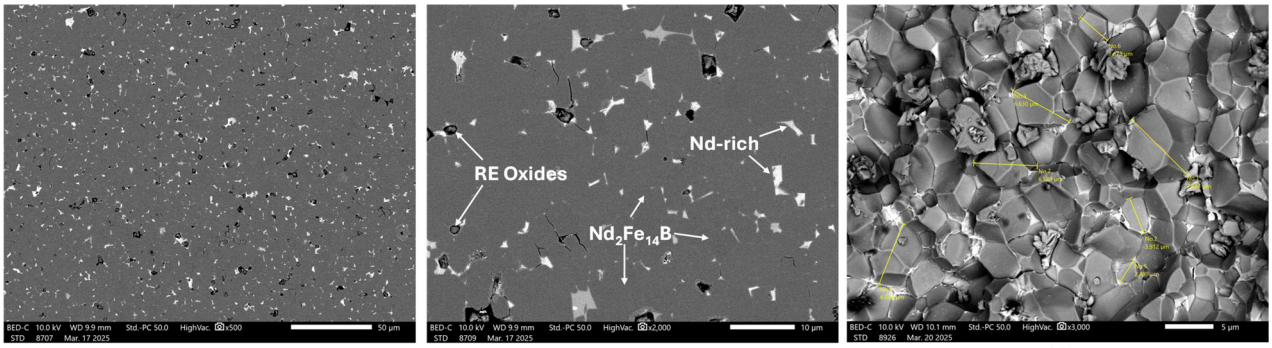

(a) (b) (c)

Fig. 2. EM magnet: (a) low-magnification microstructure, (b) high-magnification microstructure, and (c) fractured surface showing grain size.

True compositions of EM-magnets and recycled powders have been measured by inductively coupled plasma-optical emission spectrometry (ICP-OES). The oxygen, nitrogen, and hydrogen content were measured with and analyzer LECO model TCH-600 and the carbon with a LECO model CS-400.

For microstructural observation, the samples were ground using SiC abrasive papers and polished down to 0.04 µm SiO_2 particle size. The shape and microstructure of the recycled powders and magnets were studied via scanning electron microscopy (SEM) JEOL JSM-IT700HR instrument, equipped with energy-dispersive X-ray spectroscopy (EDS) for elemental analysis.

The magnetic properties of recycled powder were evaluated at room temperature using a vibrating sample magnetometer (VSM), Quantum Design PPMS-9T Model P525. To prepare the anisotropic sample for magnetic characterization, the recycled powder was mixed with a liquid epoxy resin that cures at room temperature, and the particles were aligned in a magnetic field of approximately 1 T. The resin was then allowed to solidify, fixing the particle orientation. The results were corrected to account for the effect of the demagnetizing field. To measure the magnetic properties of the initial EM-magnets and SPS-fabricated magnets, a pulse magnetizer (M-Pulse magnetizer, Magnet-Physik) was used to saturate the samples magnetically. Subsequently, the demagnetization curves were measured with a Permagraph-L from Magnet-Physik at 300 K.

3 Results

3.1 Initial magnet characterization

Table 1 provides the chemical composition and impurity content of the EM-magnets. The magnet contains a total of 28.7% rare-earth (RE) elements, with 27.2% consisting of light rare-earth (LREs) elements and 1.5% of heavy rare-earth (HREs) elements, mainly dysprosium (Dy). It's crucial to control impurity levels during the recycling process to ensure the final magnetic properties meet the desired values. One key impurity is oxygen, which can lead to the formation of unwanted oxides during recycling, potentially impacting both the microstructure and magnetic performance. The reported oxygen content (800 ppm) is high. This could affect the recycling process and final magnet properties, especially by interfering with hydrogen absorption during HD.

Similarly, the carbon content (790 ppm) is another important impurity. Excessive carbon can result in carbide formation, which could compromise the final magnet's magnetic properties. Too much carbon content could impede the sintering process, making it harder to consolidate the material properly and ultimately reducing its magnetic performance. Therefore, minimizing both oxygen and carbon content during the recycling process is crucial to optimize the 2081 magnetic properties of the recycled magnet.

Figure 2 illustrates the microstructure of the sintered Nd-Fe-B EM magnet. In Figure 2a, a homogeneous distribution of the intergranular phase can be observed, which is essential for providing effective magnetic isolation between grains and improving coercivity. Figure 2b identifies the primary phases present in the microstructure: the Nd-rich phase, the matrix phase ($Nd_2Fe_{14}B$), and rare-earth oxides, the latter typically appearing with a spherical morphology due to their formation during the sintering process. The presence of these oxides is common and can slightly influence the magnetic properties by affecting grain boundary characteristics. Minor porosity is also evident, which is typical in sintered magnets and can arise from incomplete densification or gas entrapment during processing. Finally, Figure 2c shows the fractured surface of the magnet. It highlights the grain morphology, with grain

sizes ranging from about 2.5 to 8 µm. This range aligns with the desired microstructural refinement, balancing high coercivity and remanence in these materials.

Regarding the magnetic proprieties of the EM-magnet, the measured coercivity (H_{cj}) of 1274 kA/m, remanence (B_r) of 1.345 T, and maximum energy product (BH_{max}) of 327.7 kJ/m^3 reflect a well-optimized microstructure and composition. The relatively high coercivity is supported by the presence of 1.5 wt.% Dy, which is known to preferentially segregate at grain boundaries, enhancing magnetic isolation and hindering domain wall movement. The uniform distribution of the intergranular Nd-rich phase observed in the microstructural analysis (Fig. 2a) contributes to this effect. The fine grain size, ranging from 2.5 to 8 µm, also plays a key role in achieving this coercivity by increasing grain boundary area and reducing the likelihood of reverse domain nucleation. Additionally, the presence of 1 wt.% Co may contribute to improved temperature stability. The minor additions of Cu, Ga, and Al (0.79 wt.% in total) are beneficial for promoting more uniform diffusion processes during sintering and contributing to stable grain boundary structures. Although small amounts of impurities (790 ppm C and 800 ppm O) are present, their content remains within acceptable ranges that do not significantly degrade the magnetic properties.

3.2 Powder production

Figure 3 shows the pressure variation as a function of time for different initial hydrogen pressures during the hydrogen decrepitation process. It is clear that increasing the initial hydrogen pressure reduces the activation time of the material and accelerates the reaction rate. For initial pressures of 40 and 50 bar, the pressure-time curves reach a plateau. This indicates complete hydrogenation of the material under these conditions in relatively short times: 20 min for an initial pressure of 50 bar, and up to 35 min when the initial pressure decreases to 40 bar. Additionally, the material absorbs more hydrogen at an initial pressure of 50 bar. This is due to higher hydrogen availability and a stronger driving force for diffusion at elevated pressures, which facilitates deeper penetration and a more complete reaction throughout the magnet structure.

On the other hand, for lower initial pressures (20 and 3 bar), no plateau is observed within the studied times, indicating incomplete hydrogenation of the material. This suggests that under these conditions, either the hydrogen absorption is limited by diffusion constraints or the lower driving force results in partial reaction, requiring longer times or higher pressures to achieve full hydrogenation.

Since excessively high hydrogen pressures could pose challenges at an industrial scale, hydrogen pressures of 20 and 3 bar were selected for further processing. A series of experiments were conducted to achieve complete decrepitation of the magnets under these conditions. The results showed that at 20 bar, full reaction was achieved within 1 h, whereas at 3 bar, a significantly longer reaction time of 4 h was required to reach complete decrepitation.

Figure 4 illustrates the morphology of the powder obtained at different pressures. As shown in Figures 4a and 4c, the powder exhibits an irregular shape, with particles of

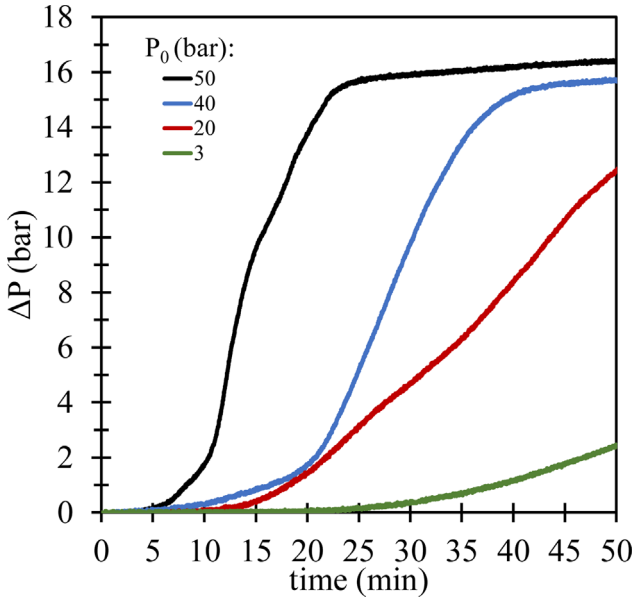

Fig. 3. Pressure variation as a function of time for different initial H_2 pressures during hydrogen absorption.

varying sizes resulting from fragmentation during the hydrogenation of the material. When the magnet is exposed to hydrogen, two reactions occur: first, the Nd-rich phase is converted into a hydride, and second, hydrogen is interstitially absorbed into the $Nd_2Fe_{14}B$ matrix phase. Both hydride formations induce volumetric expansion, with the expansion caused by Nd-rich phase being more significant.

Figure 4b shows the surface of a particle from the powder decrepitated at 3 bar. The fracture is primarily intergranular, but there is also evidence of intragranular fragmentation in this sample (indicated by arrows). This intragranular fragmentation was not observed in the powder decrepitated at 20 bar (Fig. 4d).

This suggests that at lower pressures (3 bar), the fragmentation process is more complex, involving both intergranular and intragranular fracture mechanisms, whereas at higher pressures (20 bar), the fracture is predominantly intergranular.

These differences in fracture behavior are due to variations in hydrogen absorption and the resulting volumetric expansion. At 3 bar, hydrogen absorption is less efficient and slower. This leads to less uniform expansion and higher internal stresses, facilitating both intergranular and intragranular fractures. In contrast, at 20 bar, hydrogen absorption is more uniform, causing faster expansion that primarily induces intergranular fractures.

A chemical analysis and impurities analysis was carried out on the decrepitated powder (HD-20), and the results are presented in Table 2. As can be seen, the chemical composition is very similar to that of the original magnet (Tab. 1), with a slight loss of Nd and Pr. Overall, a loss of less than 1 wt.% of Nd-Pr was observed. This minimal loss is primarily due to the hydrogenation of the Nd-rich phase during the decrepitation process, which leads to volume expansion and intergranular fragmentation. This results in

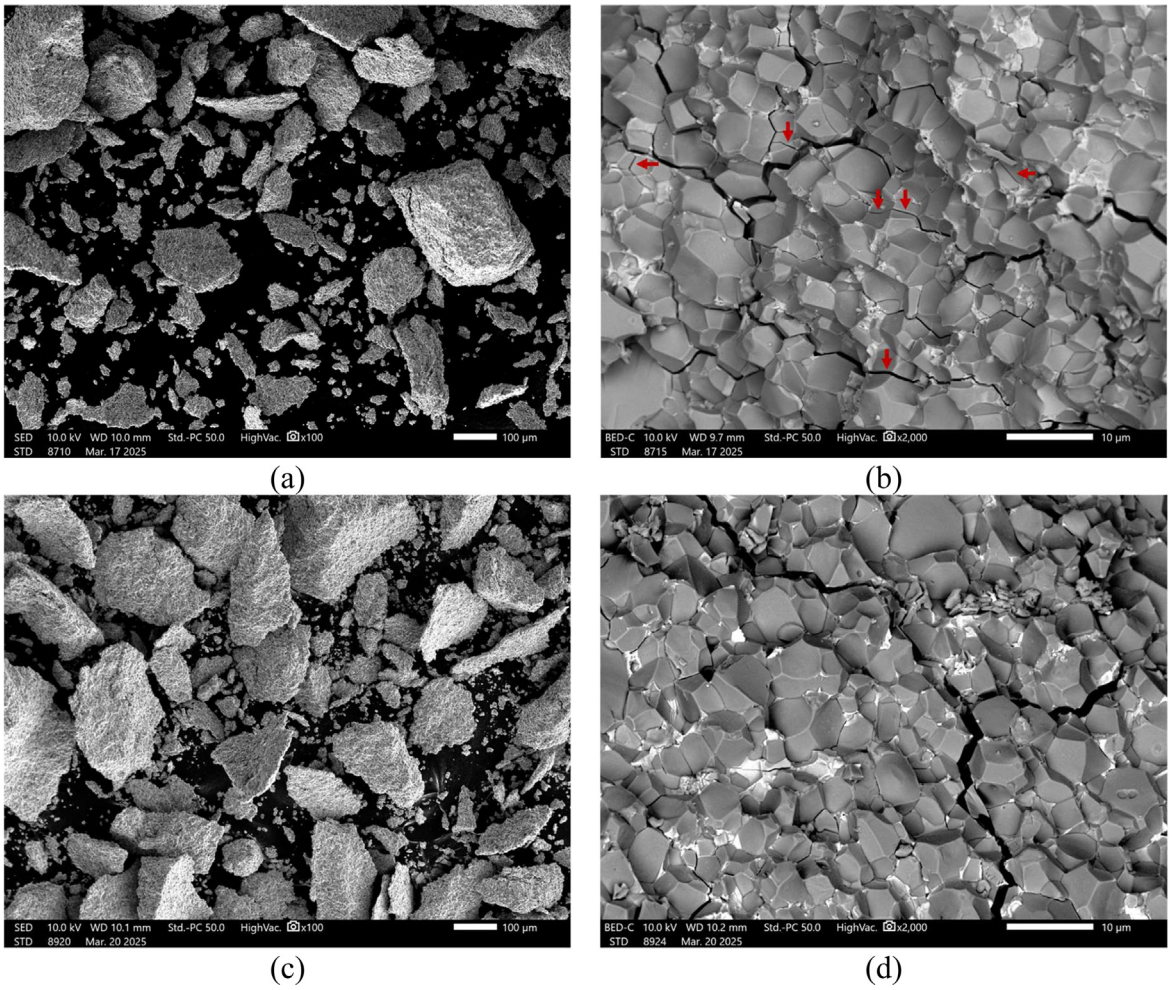

Fig. 4. SEM images of decrepitated powders at different hydrogen pressures (a, b) 3 bar, and (c, d) 20 bar. Intragranular fracture marked with red arrows.

Table 2. Chemical composition and impurity content of HD and HD-D powders.

Sample	(wt.%)								(ppm)		
	Nd	Pr	Dy	Fe	Co	B	Cu+Ga+Al	Total RE	C	O	H
HD-20	19.6	6.8	1.5	63	1.0	1.0	0.77	27.9	820 ± 30	4700 ± 300	5000 ± 200
HD-D-20						–			840 ± 10	1870 ± 30	24 ± 1
HD-D-3						–			840 ± 10	1950 ± 50	28 ± 1

the loss of some of the Nd-rich phase that is detached. However, it is worth noting that this loss is minimal. The table shows a high oxygen content in the HD material (4700 ppm after decrepitation). This is because the material reacts immediately with oxygen, even during the chemical analysis. This high oxygen content reveals the powder's high reactivity, which is attributed to two main factors: the increased specific surface area of exposed material and the reduced oxidation resistance of the hydrogenated material [14–16].

Table 2 also shows the impurities in powders obtained after dehydrogenation of decrepitated powders at 20 and 3 bar, respectively (HD-D-20 and HD-D-3). After dehydrogenation, hydrogen content is clearly reduced, while carbon content remains almost constant. The lower oxygen content in the dehydrogenated sample (HD-D-20) compared to the decrepitated powder (HD-20) is attributed to the higher susceptibility of the hydrogenated powder to oxidation when is air-exposed for analysis.

The hysteresis cycles of the HD-D-20 and HD-D-3 powders were measured along both the parallel and perpendicular axes relative to the magnetization direction. As shown in Table 3, the remanence value along the parallel axis is higher than that along the perpendicular axis (0.9 T compared to 0.71 T for the HD-D-20 sample), confirming that the obtained powder is anisotropic.

Table 3. Magnetic properties of HD-D-20 and HD-D-3 powder samples measured along parallel and perpendicular axes. Powder fraction <425 µm.

Sample	$H_{cj} \parallel$ (kA/m)	$M_r \parallel$ (T)	$M_s \parallel$ (T)	$M_r \parallel / M_s \parallel$	$H_{cj} \perp$ (kA/m)	$M_r \perp$ (T)	$M_s \perp$ (T)
HD-D-20	728.63	0.90	1.47	0.61	771.88	0.71	1.47
HD-D-3	682.22	0.90	1.46	0.62	727.49	0.73	1.45

Fig. 5. Magnet remanufactured by SPS.

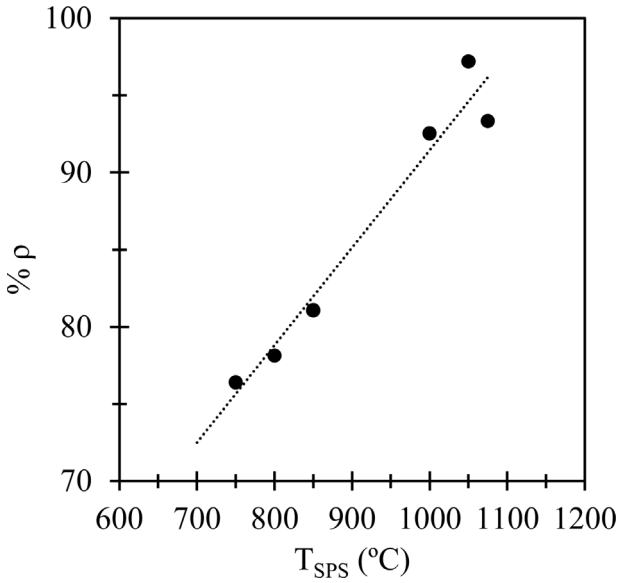

Fig. 6. Relative density (%ρ) of recycled magnets as a function of SPS holding temperature (holding time 2 min).

This anisotropy is further supported by the Mr/Ms ratio, where a value greater than 0.5 indicates a directional dependence of the magnetic properties. Specifically, values of 0.61 and 0.62 for the HD-D-20 and HD-D-3 samples, respectively, confirm the powder's anisotropic nature. Furthermore, the coercivity of the HD-D-3 powder is slightly lower than that of HD-D-20, which can be attributed to several factors, including the lower oxygen content in the HD-D-20 sample and the differences in the fracture types previously discussed.

Nevertheless, the coercivity of the powders is noteworthy, with values nearing 700 kA/m (as seen in Tab. 3). These coercivity values are competitive with those of commercial Nd-Fe-B powder [17], indicating that the recycled powder retains robust magnetic properties. This is particularly significant given that the powder is not only recycled but also exhibits anisotropy, a characteristic crucial for high-performance magnets.

3.3 Remanufacture of magnets by SPS

As shown in Figure 5, an example of a remanufactured specimen obtained via SPS is presented. The specimens were fabricated using both directly decrepitated powder (HD) and decrepitated and dehydrogenated powder (HD-D).

Figure 6 presents the relative density of recycled magnets obtained by SPS, assuming a theoretical density of 7.5 g/cm^3. Relative density of the recycled magnets increases from approximately 75% at 750 °C to over 90% for sintering temperatures above 1000 °C, reaching a maximum value close to 98% at 1050 °C. Nevertheless, it is noteworthy that this high densification has been achieved with a very short holding time of only 2 min during the SPS process, highlighting the efficiency of spark plasma sintering in promoting rapid consolidation.

Since the highest density value was obtained for the sample sintered at 1050 °C for 2 min, these conditions were used to manufacture recycled magnets via Spark Plasma Sintering (SPS RM) using the HD-20 decrepitated powder samples (SPS RM-1) and the dehydrogenated HD-D-20 samples (SPS RM-2), as well as HD-D-3 (SPS RM-3).

Figure 7 shows the microstructure of a specimen obtained by Spark Plasma Sintering (SPS RM-03). Figure 6b identifies the primary phases present in the microstructure: the Nd-rich phase, the matrix phase ($Nd_2Fe_{14}B$), and rare-earth oxides. The presence of these oxides was also observed in the EM magnet but the amount is higher in the SPS samples. This can slightly influence the magnetic properties by affecting grain boundary characteristics. The oxygen content of the specimens after SPS (SPS RM-03) was 2180 ± 40 ppm. This value is slightly higher than the measurement in the initial powder (HD-D-03). This increase may be due to contamination during the sintering process. This value is also higher than that of the original EM magnet (800 ppm).

The carbon content after the SPS process was 980 ± 10 ppm, which is slightly higher than both the initial powder and the original magnet. This is an interesting aspect, as the tooling used during the SPS process (dies, punches and foils) are made of graphite and may be causing slight contamination in the internal part of the magnet. The surface of the sample was removed for the chemical analysis.

Figure 7c shows the fractured surface of the magnet, highlighting the grain morphology with grain sizes ranging from approximately 4 to 9 µm Compared to the original EM

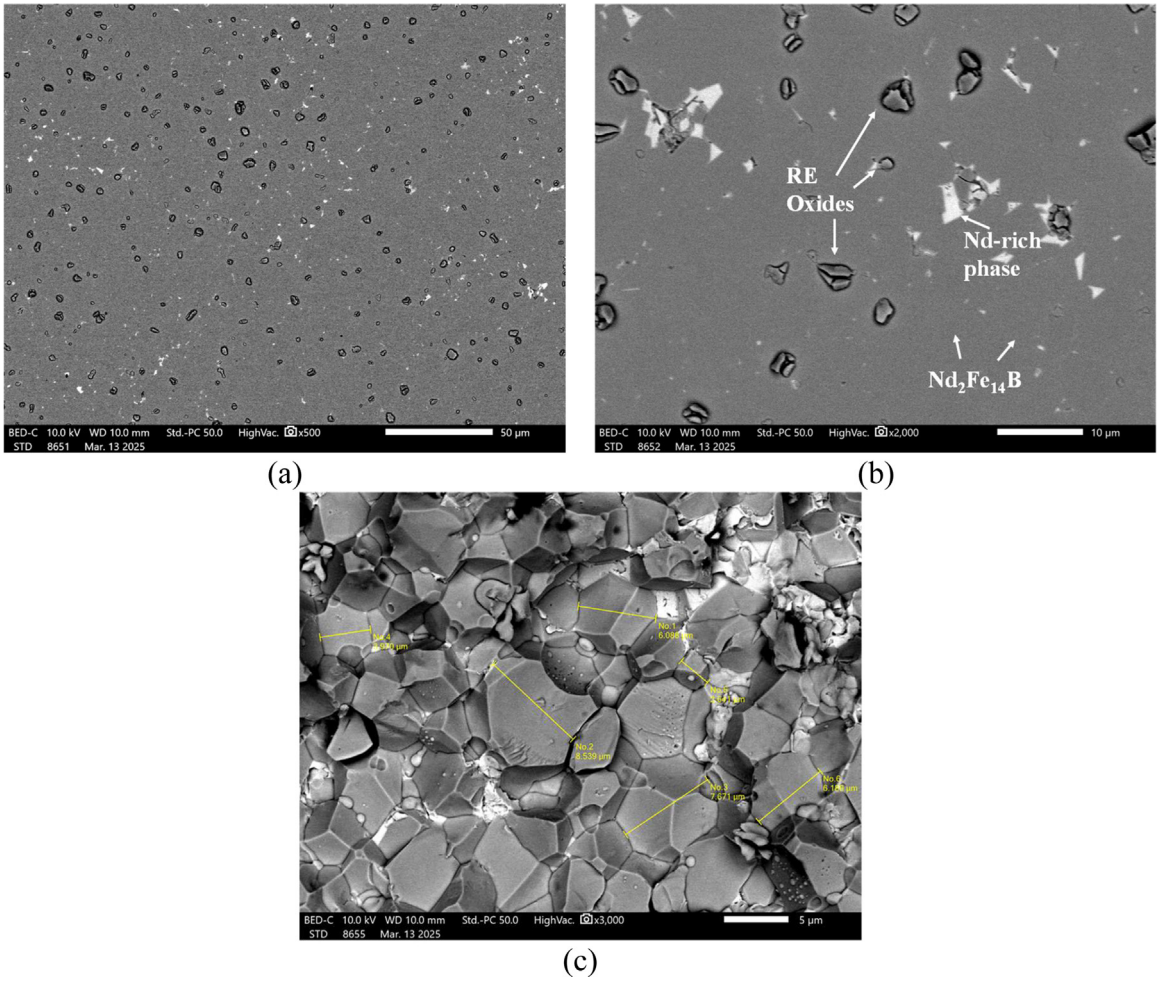

Fig. 7. SPS RM-3: (a) low-magnification microstructure, (b) high-magnification microstructure, and (c) fractured surface showing grain size.

magnet, the grain size is similar or slightly larger, but more statistical analysis would be needed to confirm this observation as the difference is very small.

Regarding the magnetic properties of the sintered magnets, Figure 8 shows the demagnetization curves of different magnets, and Table 4 includes the detailed magnetic properties.

The specimens obtained via SPS using HD powder (decrepitated but not dehydrogenated) exhibit very low magnetic properties because the SPS thermal cycle is not capable of removing the hydrogen present in the material.

Among the specimens obtained using dehydrogenated powder (HD-D-20 and HD-D-3), there is no significant difference between powder decrepitated at 3 bar or 20 bar. When comparing the specimens obtained after SPS sintering with the properties of HD-D-3 and HD-D-20 powders, it can be indicated that coercivity and remanence have decreased by about 15%. This is likely due to a slight increase in grain size and minor contamination with oxygen and carbon. These changes occur during the SPS process, which is performed under low vacuum and in the presence of graphite.

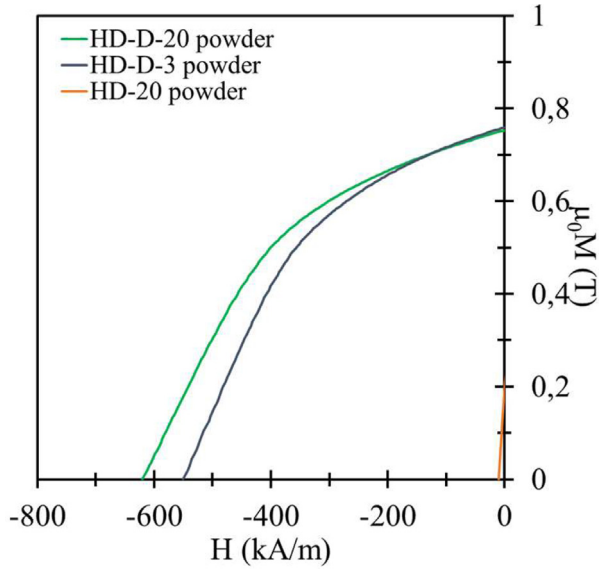

Fig. 8. Demagnetization curve of SPS recycled magnets.

Table 4. Magnetic properties of SPS recycled magnets fabricated with powders HD-D-20 and HD-D-3 at 1050 °C.

Sample	Powder	ρ (g/cm^3)	% ρ	H_{cj} (kA/m)	H_{cb} (kA/m)	M_r (T)	BH_{max} (kJ/m^3)
SPS RM − 1	HD-20	7.29	97.2	10.1	9.58	0.1930	0.54
SPS RM − 2	HD-D-20	7.31	97.5	622.4	401.0	0.7576	84.47
SPS RM − 3	HD-D-3	7.37	98.2	548.3	371.7	0.7574	81.09
SPS-ref	MQ	7.36	98.1	811.7	491.4	0.7306	90.87

Regarding the anisotropy of the magnets, no magnetic orientation of the powder was performed in these samples, so a significant anisotropy is not expected. However, the remanence values measured in the SPS RM-2 and SPS RM-3 magnets with HD-D powder are slightly higher than the remanence values measured perpendicular to the easy axis of magnetization in the powder (0.71 and 0.73, respectively). This could be an indicator of some residual anisotropy in the magnet (although it is very small), which is due to the anisotropic nature of the powder particles. Some of this anisotropy transfers to the magnet, even though the particles were not pre-oriented before the sintering process. This occurs simply due to the preferred alignment of the particles caused by their morphology.

For comparison, a magnet was also obtained via SPS using commercial melt-spun powder from Magnequench, sintered at 850 °C (labeled as SPS-ref in Tab. 4), with all other conditions identical to those used in this study. The magnetic product (BH_{max}) obtained with the recycled powders is quite similar to that achieved with the commercial powder. The main difference lies in the coercivity, which is higher for the commercial melt-spun powders due to their smaller grain size. Very similar results have been reported in other studies involving isotropic magnets produced via SPS [18]. The magnets obtained are still far from the commercial magnets with the best properties. Commercial anisotropic magnets can achieve BHmax values exceeding 300 kJ/m^3 and very high coercivity [19]. However, it is important to note that the magnets developed in this work are isotropic. Further research is needed to orient the particles to achieve properties comparable to high-quality commercial magnets.

4 Conclusions

In this study, an innovative process has been developed that combines the use of HD (decrepitated) powders with Spark Plasma Sintering (SPS). This short-cycle process allows for the rapid recovery of magnets, which is a significant advantage in terms of efficiency and sustainability. The advantages of the developed recycling process (HD powders + SPS) include the use of low-cost HD powders, as the processing required to obtain them is simple and quick, especially at high pressure. Additionally, these powders are less reactive due to their particle size and retain some anisotropy, which benefits their magnetic properties. The pressure during decrepitation plays a critical role in determining the fracture mode, with lower pressures promoting more intricate fragmentation due to uneven expansion, and higher pressures favoring intergranular fracture due to more controlled material deformation.

The magnetic properties of the recycled magnets are moderate compared to the EM magnet, but it is important to note that the developed magnets are isotropic. Their properties are comparable to those of isotropic magnets produced via SPS using primary material.

This work represents a first step in the development of cost-effective recycled magnets by SPS, and there are several possibilities for improving the performance of the magnets. The first is the alignment of the magnets before the SPS cycle, which can introduce anisotropy into the material and enhance magnetic properties. Another potential improvement is the addition of rare earth elements to compensate for the losses incurred during recycling. Annealing treatments could also be used to improve the intergranular phase distribution. These enhancements could further enhance the magnetic properties and overall performance of the recycled magnets.

From an environmental perspective, the proposed solution offers two key advantages: the use of recycled materials, which significantly reduces resource extraction and associated impacts compared to virgin feedstocks, and the implementation of energy-efficient FAST sintering, which outperforms conventional vacuum furnace methods in terms of energy consumption. However, quantifying the exact environmental contribution of these innovations requires a comprehensive life cycle assessment (LCA) to account for all stages of production, transportation, and end-of-life processes. Such an analysis, while beyond the scope of this study, would provide precise metrics to validate the sustainability benefits at scale.

Acknowledgments

We would like to express our gratitude to Orona S. Coop for their generous donation of elevator motors and magnets, which were essential for completing this study.

Funding

This work has been funded by the Basque Government through the project ELKARTEK CIPEME (KK-2024/00053).

Conflicts of interest

The authors have nothing to disclose.

Data availability statement

This article has no associated data generated and/or analyzed.

Author contribution statement

Conceptualization, M.A. Lagos, B.L. Checa; Methodology, J.M. Sanchez; Validation, J. Poza, G. Almandoz, A. Escalada; Investigation, M.A. Lagos, I. Leizaola, B.L. Checa, J. M. Sanchez; Writing – Original Draft Preparation, B.L. Checa, M.A. Lagos; Writing – Review & Editing, all; Supervision, I. Agote; Project Administration, M.A. Lagos; Funding Acquisition, M. Lagos, I. Agote.

References

1. Q. Lu, Y. Shao, Y. Yin et al., Mass production of regenerated sintered NdFeB magnets with improved magnetic properties compared to original magnets, Sustain. Mater. Technol. **36**, 2476 (2023)
2. N.A. Mancheri, B. Sprecher, G. Bailey et al., Effect of Chinese policies on rare earth supply chain resilience, Resour. Conserv. Recycl. **142**, 101 (2019)
3. P. Chen, E.S. Ilton, Z. Wang et al., Global rare earth element resources: a concise review, Appl. Geochem. **175**, 106158 (2024)
4. A.M. Dickinson-Lomas, M.J. Keith, D.N. Brown et al., The removal of epoxy resins from NdFeB magnets for recycling-a review, Resour. Conserv. Recycl. **108**, 108113 (2025)
5. D. Talan, Q. Huang, A review of environmental aspect of rare earth element extraction processes and solution purification techniques, Miner. Eng. **176**, 107430 (2022)
6. P. Zapp, A. Schreiber, J. Marx et al., Environmental impacts of rare earth production, MRS Bull. **47**, 267 (2022)
7. F. Xiao, W. Hu, J. Zhao et al., Technologies of recycling REEs and Iron from NdFeB Scrap, Metals **13**, 779 (2023)
8. I.R. Harris, P.J. McGuiness, Hydrogen: its use in the processing of NdFeB-type magnets, J. Appl. Phys. **64**, 5308 (1988)
9. B.L. Checa Fernández, J.M. Martín, G. Sarriegui et al., Effect of temperature on particle shape, size, and polycrystallinity of Nd-Fe-B powders obtained by hydrogen decrepitation, J. Mater. Res. Technol. **24**, 1454 (2023)
10. A. Walton, H. Yi, N. Rowson et al., The use of hydrogen to separate and recycle neodymium-iron-boron-type magnets from electronic waste, J. Clean. Prod. **104**, 236 (2015)
11. B. Sprecher, Y. Xiao, A. Walton et al., Life cycle inventory of the production of rare earths and the subsequent production of NdFeB rare earth permanent magnets, Environ. Sci. Technol. **48**, 3951 (2014)
12. T. Tomše, Microstructure refinement of Nd-Fe-B permanent magnets prepared via spark-plasma sintering, IEEE Trans. Magn. **60**, 1 (2024)
13. T. Tomše, Z. Samardžija, L. Scherf et al., A spark-plasma-sintering approach to the manufacture of anisotropic Nd-Fe-B permanent magnets, J. Magn. Magn. Mater. **502**, 166504 (2020)
14. T. Chun-Lin, B. Shu-Xin, Z. Hong et al., Effects of hydrogen on the oxidation of coarse decrepitated powder of Nd-Dy-Fe-B alloy, J. Alloys Compd. **368**, 333 (2004)
15. J. Tejada, J.M. Hernandez, M. Duran et al., The effect of hydrogen on the magnetic properties of the Nd-Fe-B-H compound, J. Magn. Magn. Mater. **195**, 476 (1999)
16. A.J. Williams, P.J. McGuiness, I.R. Harris, Mass spectrometer hydrogen desorption studies on some hydrided NdFeB-type alloys, J. Less Common Met. **171**, 149 (1991)
17. Magnequench, https://mqitechnology.com/products/ (2023)
18. M. Keszler, F. Grosswendt, C. Assmann et al., Direct recycling of hot-deformed Nd-Fe-B magnet scrap by field-assisted sintering technology, Adv. Energy Sustain. Res. **5**, 2300184 (2024)
19. Stanford Magnets. (2024, April 16). Bonded NdFeB magnets vs sintered NdFeB magnets. Retrieved July 15, 2025, from https://www.stanfordmagnets.com/

Cite this article as: Miguel Lagos, Blanca Luna Checa Fernández, Iñaki Leizaola, Jon Mikel Sanchez, Iñigo Agote, Gaizka Almandoz, Javier Poza, Ana Escalada, Short-loop recycling of elevator motor magnets by hydrogen decrepitation and FAST sintering, Metall. Res. Technol. **122**, 601 (2025), https://doi.org/10.1051/metal/2025075